USGS Award G16AP00116

Procedures for Using UCERF3 in Site-Specific Seismic Hazard Analyses in California

John G. Anderson

Nevada Seismological Laboratory, MS104
    University of Nevada, Reno
    775-784-1954
    jga@unr.edu

Glenn P. Biasi

U. S. Geological Survey
    Pasadena
    gbiasi.seismo@gmail.com

Abstract

The hazards community is looking for guidance on how to use UCERF3 in site-specific hazard assessments. Even experienced site hazard analysts find the model challenging. Questions that arise when attempting to apply UCERF3 include how to isolate relevant ruptures, rates, and uncertainties, how to adapt the solution to different epistemic uncertainties in slip rate, and how to incorporate projectspecific geologic information or alternative epistemic uncertainties. In addition a practical way to deaggregate the UCERF3-based model is needed for site-specific understanding of hazard contributions. Deaggregation resources have been available for previous models, and are used to address a variety of hazard-related questions.

In this project we proposed to develop:

1. Practical procedures for deaggregating the fault source component of the California seismic hazard as estimated by UCERF3. The process will be provided in a working form and readily implemented in a USGS-hosted computational platform such as OpenSHA.

2. Tools to extract unique rupture sets for site-specific applications from the UCERF3 model. These rupture sets will be suitable for import into private hazard codes being used by the hazard community.

3. Processes for recovering rupture rate uncertainties when needed.

4. Methods for integration of project geotechnical study that affect estimates or uncertainties in fault geometry or slip rate beyond what is included in the UCERF3 model.

Procedures developed in this proposal are intended to improve the professional interface between the NSHMP and the California user community. Under this project, objectives 1-3 have been fully achieved, and with the tools that have been developed, the informed user will be able to easily substitute an updated description of fault properties that result from geotechnical studies.

Report

Initial work related to this project and completed before the project was awarded resulted in a publication by Biasi and Anderson (2016) that demonstrated how UCERF3 can be deaggregated efficiently.

We have applied this method, with extensions to consider the uncertainties in seismicity rates that are incerent in UCERF3, to find examples of the impact of those uncertainties on hazard estimates. These results (Anderson and Biasi, 2018a) are described in Appendix A.

We have prepared an efficient code in the Matlab platform that can be used to achieve the deaggregation that is described by Biasi and Anderson (2016). This code is described in Appendix B. It is our hope that the code is a big step toward putting UCERF3 in fine detail into the hands of the local hazard practitioner.

Anderson (2018) has also considered, with partial support of this grant, the uncertainties in the seismic hazard as they affect the Reno-Carson City - Lake Tahoe urban region.

Bibliography

Anderson, J. G. (2018). Quantifying the epistemic uncertainty in the probabilistic seismic hazard from two major faults in western Nevada, Earthquake Spectra (Available as a preprint on the Earthquake Spectra web site in April, 2018).

Anderson, J. G. and G. P. Biasi (2018a). Examples of Sensitivity of Hazard Estiamates to Uncertainties in the UCERF3 Seismicity Model (Appendix A).

Anderson, J. G. and G. P. Biasi (2018b). UCERF3 Explorer 1: Software For Engineers (Appendix B).

Biasi, G. and J. G. Anderson (2016). Disaggregating UCERF3 for Site-Specific Applications, Earthquake Spectra 32, 2009-2026.

Appendix A

Examples of Sensitivity of Hazard Estimates to Uncertainties in the UCERF3 Seismicity Model

John G. Anderson and Glenn P. Biasi

August 31, 2018

Abstract

UCERF3 implements an innovative new procedure to characterize the rupture rates of potential on-fault earthquakes in California. The rupture rates are the result of an inversion process that incorporates constraints from historical seismicity, geological studies of fault geometry, slip rates, slip per event, and recurrence intervals, and geodetic observations of regional deformation rates. We extend this rate analysis to find the magnitude-frequency distribution (MFD) on the smallest unit scale of UCERF3, the fault subsection. The inversion is highly under-determined so 10 runs are averaged to produce rupture rates for each of the 720 logic tree branches of a given fault model. We illustrate sensitivities with fault model FM3.1. MFD solutions vary among branches by one to three orders of magnitude on individual subsections. Using the efficient approach of Biasi and Anderson (2016) to calculate the seismic hazard, this paper subsequently explores hazard estimates from each of the 720 MFDs for four diverse sites in California.

In spite of the variability of the branch MFDs, hazards from the ensemble for individual subsections of faults are much more stable, generally showing a range of a factor of ~5 or less in exceedance rates at a given level of ground motion. When multiple subsections are combined, the variability may decrease even more. In the end, at three of the four considered sites, the uncertainty in ground motion at the exceedance rate of 2% in 50 years due to the on-fault seismicity model is comparable to the uncertainty due to the ground motion prediction equations. This result is very encouraging for probabilistic seismic hazard analysis, at least in regions such as California where sufficient geophysical constraints are available to build models of the seismicity.

1 Introduction

As with any field of science that impacts the general public, it is important for seismic hazard analyses to understand the uncertainties in their models. In support of this goal, many recent studies of seismic hazard have described the

sensitivity of the models to uncertain parameters in the input to the hazard (e.g. Rabinowitz and Steinberg, 1991; Rabinowitz et al., 1998; Grünthal and Wahlström, 2001; Beauval and Scotti, 2004; Sabetta, et al., 2005; Barani et al., 2007; USNRC, 2012; Molkenthin et al., 2015, Yasdani et al., 2016; Omang et al., 2016; Matan et al., 2017; Molkenthin et al., 2017; Anderson, 2018; Lee et al., 2018). Anderson (2018) summarized the approach used in most of these studies. However, although it has been in use for four years, now, there has not been much attention paid to uncertainties in hazard estimates that result from uncertainties in the Uniform California Earthquake Rupture Forecast, Version 3 (UCERF3) beyond that provided as part of the orignial documentation of the model (Field et al., 2013; 2014).

UCERF3 represents the seismicity component in the 2014 National Seismic Hazard Model (Petersen et al., 2014). UCERF3, described by Field et al (2014), implements an innovative new procedure to characterize earthquakes on the faults in California. The model uses two geometries, FM3.1 and FM3.2, to represent the epistemic range in fault geometries. In FM3.1, which is the simpler of the two, the faults are characterized by 2606 subsections with a distribution of map lengths that have mean of 6.2 km and standard deviation of 1.8 km. The full range of subfault lengths is from 1.7 km to 15.1 km, but most are between 4.2 and 7.4 km in length. Most of these subfaults extend from the surface to the base of the seismogenic zone, the most common value of which is 13 km. Possible ruptures are identified by joining between two and 211 adjacent subsections to create a list of 253,706 possible earthquake ruptures. Branch-averaged mean magnitudes of these ruptures range from 5.08 to 8.34. The distribution of the number of subsections per rupture peaks between 16-20 subsections. The rate of each of these possible ruptures is estimated from an inversion, using simulated annealing, that incorporates constraints from historical seismicity, geological studies of fault geometry, slip rates, slip per event, and recurrence intervals, and geodetic observations of regional deformation rates (Field et al., 2014). This approach relaxes assumptions of fault segmentation and allows for multi-fault ruptures. The absence of these possibilities in UCERF2 (e.g. WGCEP, 2007) has been increasingly recognized as problematic when viewed from the perspective of large earthquakes worldwide (Field et al., 2014).

Individual UCERF3 inversion runs that fit geological and geophysical constraints typically estimate rates for between 7,000 and 11,000 ruptures. Branch rates average over 10 inversions. One question that is addressed in this paper is how effectively these constraints will stabilize the hazard estimates, in spite of the extremely underdetermined nature of the inverse problem to estimate the rupture rates. This has been addressed to some extent by Field et al. (2014), in which the supplementary online figures show the range of hazard curves determined from the different branches of the UCERF3 logic tree. This paper describes a method that can conveniently carry out such a sensitivity analysis, and extend the sensitivity to considerations associated with the ground motion prediction equations that combine with the UCERF3 model to generate hazard curves.

Considering the complexity of the model, at first it might seem that deter-

mining the sensitivity of the hazard to the UCERF3 model might be nearly intractable without a high-performance supercomputer. However, that is not the case. Biasi and Anderson (2016) presented one approach that aggregates features of the model and greatly simplifies applications. Using their approach, the contribution of faults in UCERF3 to the seismic hazard can be computed on a desktop computer in a reasonable amount of time. The Biasi and Anderson (2016) approach focuses on the individual fault subsections. In FM3.1, the median number of ruptures affecting an individual fault subsection is 168. The maximum is 167,338 of the possible ruptures. But for hazard purposes, using the NGAW2 generation of GMPEs, the hazard depends on the magnitude and the nearest approach of the fault to the station. Since the range of magnitudes is bounded, it is possible to find the combined rate of all of the possible ruptures that fall within narrow magnitude bins. For example, hundreds to thousands of ruptures that involve a single fault subsection with magnitudes between 6.0 and 8.4 can be consolidated to 24 hazard calculations using the rates of earthquakes in bins with a width 0.1 magnitude unit. Every rupture is considered, and contributes to the hazard at its appropriate distance from the site. In fact, using this method, the most time consuming part of the calculations is, for some sites, removing the duplicated ruptures from the more distant fault subsections. Biasi and Anderson (2016) called these reduced magnitude-frequency distributions for a specific site the "site-specific subsection magnitude frequency distribution", or "s3mfd". Once that is done, the hazard calculations generally proceed quickly.

Anderson (2018) recently discussed the sensitivity of the seismic hazard in the Reno area to uncertainties in the fault properties. The seismicity in Nevada is described in the traditional sense, where individual faults are identified, measured, and assigned magnitude and earthquake occurrence rates for whole-fault ruptures by applying scaling parameters and simple conversions of slip rate to occurrence rate. Sensitivity of the hazard to the seismicity model can be separated into sensitivity to slip rate, magnitude, and the simplified fault geometry. This paper extends the methods used in that application to seismicity as described by UCERF3, and applies the results at four representative sites.

2   Sensitivity Analysis Methodology

Distinct from Anderson (2018), the sensitivity analysis here is relatively simple. This paper divides the uncertainty into the contribution of only two elements of the hazard. The first is the seismicity model, which can also be called the rupture forecast in this case, as it addresses only the contribution of earthquake ruptures on known faults to the hazard. The second is the choice of ground motion prediction equations (GMPE). As in Anderson (2018), the results will be displayed using a tornado diagram.

UCERF3 uses a logic tree (Field et al., 2014) for which the fault geometries in FM3.1 or FM3.2 are the first branch. For FM3.1, and for FM3.2, the logic tree uses 720 combinations of models for the remaining properties. For the purposes of this paper, it is sufficient to consider only FM3.1. Thus, this paper

considers 720 branch-average rupture rate models, each giving an estimated annual occurrence rates of all of the 253,706 possible earthquake ruptures. As suggested by Field et al. (2014), hazard curves based on these logic tree branches are considered in this paper to sample the variability due to the seismicity.

As in Anderson (2018), this project uses four GMPEs from the NGA2 west project: Abrahamson et al. (2014), Boore et al. (2014), Campbell and Bozorgnia (2014), and Chiou and Youngs (2014). By using the average rupture rate model for FM3.1, the differences in the the ground motion resulting from these different models will be used to explore the uncertainty due to the GMPE. The average hazard curve used as reference in the tornado diagrams is the average from the hazard curves using the four GMPEs and the average rupture rate model.

The tornado diagram displays the full range of hazard relative to the reference hazard curve, ignoring branch weights. The hazard parameter characterized by the tornado diagrams is the amplitude of ground motion with annual exceedance rate of $4.04 \cdot 10^{-4}$ per year, corresponding to a probability of exceedance of 2% in 50 years on the assumption that the earthquakes in the model are Poissonian. The ground motion at this exceedance rate is used to set seismic design requirements in the International Building Code (ref). Setting a_i as the ground motion from the ith hazard curve and a_0 as the motion for the reference curve, the tornado diagram depicts the range from $\ln \left(\frac{\min\{a_i\}}{a_0} \right)$ to $\ln \left(\frac{\max\{a_i\}}{a_0} \right)$. To display the effect of the GMPE, the set $\{a_i\}$ represents ground motions from hazard curves with the average rupture rate model but different GMPEs. To display the effect of the seismicity model, the set $\{a_i\}$ represents ground motions from hazard curves with the average GMPE but different FM3.1 logic tree branches. The total variability is represented by including in $\{a_i\}$ the 2880 hazard curves from the 720 logic tree branches and 4 GMPEs.

Figure 1 shows the locations of the upper edges of fault subsections in FM3.1, one of the two geometries used in UCERF3, and the locations of the considered sites. The four sites are intended to represent different conditions. The first three sites considered here were also considered by BA16. Lovejoy Buttes is near the San Andreas fault in the Mojave Desert, and there are no other fault sources within 30 km. Long Beach Harbor has several nearby faults with moderate activity rates, while the most active faults (San Andreas, San Jacinto) are much farther away. San Jose Airport is midway between the San Andreas and Hayward faults, but also has a less active fault nearby. Finally, South Lake Tahoe is in a normal faulting environment near the California boundary, in a location where active faults to the east were outside of the scope of UCERF3.

3   Results

Results of the study are summarized in Figures 2 to 7.

3.1 Lovejoy Buttes

This site (Figure 2) is interesting because it is near the center of a cluster of precariously balanced rocks, which Brune (1999) has proposed can be used as a test of the seismic hazard analysis. The rocks can be toppled by a static acceleration of ~0.3-0.5 g. Rock ages are possibly ~10,000 years. Based on FM3.1, the annual exceedance rate of Mw7.75 earthquakes rupturing the nearest subsection of the San Andreas fault is $(4 \pm 2) \cdot 10^{-3}$ per year (Figure 8). This suggests that these rocks have potentially experienced ~40 earthquakes of Mw7.75 or larger.

The net result for Lovejoy Buttes is that the uncertainties in the hazard at this site from the GMPEs are greater than from the fault model, both for SA(1) (Figure 6a) and for peak acceleration (Figure 7a). Figure 4a shows the hazard curves for SA(1) for each of 279 subsections within 100 km of the site. The five that have the most significant contributions at ~0.25g have been highlighted. The total hazard is of course the sum of the contributions from all of the subsections. As was found by Biasi and Anderson (2016), the nearest subsection with identification number 1846 (fss1846), is the dominant contributor at this location. The other four highlighted fault subsections add ruptures that end on the San Andreas close to fss1846 but do not rupture past the site. The individual contributions of each of these other four subsections is an order of magnitude smaller than the contribution from fss1846.

Figure 4a shows the rates of earthquakes, in magnitude bins of width 0.1 magnitude, for fss1846. The average FM3.1 solution, shown by the large red points, was used to construct the hazard curves in Figure 3 Even though all of the 720 solutions are constrained to be close to matching the constraints on the seismicity, there is a large amount of variability in these distributions. The distribution for Mw7.9 is most tightly constrained, but nonetheless ranges from $(2.8 - 20.4) \cdot 10^{-4}$ per year, so there is nearly an order of magnitude of variability in the estimated rate of earthquakes of this magnitude passing the site. The various logic tree branches for other values of Mw have a range of two to three orders of magnitude in occurrence rates, Obviously, however, there are tradeoffs in rates of adjacent magnitude bins. This can be seen in the cumulative magnitude frequency distributions for these 720 curves, which converge below Mw7.8 (Figure 8).

Considering the variability in earthquake rates, it is interesting to examine the range of hazard curves at the site caused by only the nearest fault subsection. This is shown in Figure 9. This actually shows 2880 hazard curves, using 720 branches and each of the four GMPEs. The 720 branches for each of these GMPEs is shown in a different color. In this figure, the uncertainty range at low amplitudes is, by one measurement, even smaller than the range of earthquake rates. The range of rates of exceedance of SA(1) below 100 cm/s^2 vary within a factor of 2-3. This amount of uncertainty is still significant, but it is reassuring that the large variability in rupture rates is collapsed to a smaller range when processed through the hazard integral.

Figure 5a again shows 2880 hazard curves. In this case, the contributions from all of the subfaults within 100 km are included, and separate hazard curves

for each of the GMPEs are displayed. Thus the range of the gray-shade lines encompass the entire range of uncertainty that arises from the faults and GMPEs. At 100 cm/s^2, the exceedance rate estimates span a range that is a factor of 4, i.e. relative to a median value, the uncertainty in rate is +- a factor of two. This is somewhat larger than the range that arose from the nearest fault subsection, but still significantly smaller than the range of earthquake occurrence rates shown in Figure 4.

3.2   Long Beach Harbor

The several faults near the Long Beach Harbor site (Figure 2b) have a complicated geometry, and both strike-slip and reverse senses of slip are represented. The five leading contributions to the hazard at 0.25g come from five faults, as identified in Figure 3b. The nearest fault subsection (Su1517 on the Palos Verdes fault) has the strongest contribution at this amplitude, but below ~0.1g, the San Andreas fault makes the most important contribution to the hazard at 1 second oscillator period (Figure 3b). The MFD for Su1517 is strongly peaked at Mw7.3 (Figure 4b). A full fault rupture of the Palos Verdes fault causes this magnitude, but the rate of Mw7.3 $\pm$ 0.05 earthquakes is uncertain by a factor of 40. Nonetheless, the range of exceedance rate of SA at 0.25g from Su1517 is only a factor of ~5. Thus again, the integral process of finding the hazard curves smooths out the large range of earthquake occurrence rates. Figures 6b for SA(1) and Figure 7b for peak acceleration find that the uncertainty among the branches of FM3.1 make a larger contribution to the total uncertainty in the hazard in this case.

3.3   San Jose Airport

At San Jose Airport (Figure 2c), the five main contributions to the hazard at ~0.25g come from three major regional faults: the Hayward, Calaveras, and San Andreas faults (Figure 3c). The nearest fault subsection (Su2386 on the Silver Creek fault) makes an insignificant contribution to the total. The MFD for Su2386 is nonetheless shown in Figure 4c, as it is the nearest fault to the site. This MFD is peaked at Mw6.0, for which the rate is ~3.8e-5 per year, which is only about 2% of the rate of earthquakes on the most important subsection of the Hayward fault. From the set of hazard curves in Figure 5c, the range of exceedance rates of SA at 0.25g from all contributing subfaults spans a factor of ~5. In the tornado diagram (Figure 6c), the uncertainty due to the GMPE is substantially greater than the uncertainty from the various branches of the logic tree. Considering that the uncertainty due to the GMPE at the San Jose Airport site is comparable to the uncertainty at the other sites, we interpret this to result from the many constraints available on the behavior of the main faults.

3.4 South Lake Tahoe

The South Lake Tahoe site (Figure 2d) is located between the surface traces of the West Tahoe fault and the Carson Range fault. The site is on the hanging wall of the West Tahoe fault. Figure 3d finds that the the three nearest subsections of the West Tahoe fault and the two nearest subsections of the Carson Range fault constitute the five strongest contributions to the hazard at ~0.25g. The Mw6.7 event that is the most probable rupture in Figure 4d involves the nearest subsection (Su2545) and the two subsections to the south along the West Tahoe fault. Figure 5d, showing all of the considered hazard curves, indicates that the uncertainty is larger than for the other three sites. This is confirmed by the tornado diagram in Figure 6d. The uncertainty due to the GMPEs is not a lot different from the other three sites, but the uncertainty arising from the branches of the logic tree in FM3.1 is considerably larger than it is at the other three sites in this figure. Comparison with the USGS 2014 hazard curve (Petersen et al., 2014) indicates that these two faults do not contribute all of the total hazard at exceedance rates of $4 \cdot 10^{-4}$ per year and smaller. Several factors are involved. The total USGS hazard curve includes faults farther to the east, which are not included in UCERF3, but are considered by the USGS. Besides this, there is a substantial uncertainty in which faults at this latitude take up the total deformation in the Walker Lane (e.g. Wesnousky et al., 2012). To accomodate this lack of knowledge, the hazard in this area has a stronger contribution from background seismicity than at the other considered locations.

4 Conclusions

UCERF3 demonstrates a large amount of uncertainty in the occurrence rates on a single fault, as shown in Figure 4. In spite of this, hazard estimates show a much smaller uncertainty range. Thus the integration process that generates a hazard curve from the seismicity model has a strong smoothing effect. This is very reassuring, as it demonstrates that the hazard estimates are a relatively stable function as a result of the constraints on the seismicity models.

In the examples presented in this paper, the contribution of the GMPE to the total uncertainty is less variable that the contribution from the faulting model. At the two locations where the faulting model is relatively well constrained, such as the two considered sites close to the San Andreas fault, the hazard is more sensitive to the GMPE than to the faulting model. On the other hand, at the two sites with less active local faults dominating the hazard, the uncertainties associated with those faults are larger than the uncertainties due to the GMPEs.

Perhaps the most important point of this paper, however, is that we have developed a package of software that can efficiently provide estimates of the uncertainties in the hazard for locations in California. The codes are available from the authors at this time.

5   Acknowledgements

6   References

Abrahamson, N. A., Silva, W. J., and Kamai, R. (2014). Summary of the ASK14 ground motion relation for active crustal regions. Earthquake Spectra, 30(3):1025–1055.

Anderson, J. G. (2018). Quantifying the epistemic uncertainty in the probabilistic seismic hazard from two major faults in western Nevada, Earthquake Spectra (Available as a preprint on the Earthquake Spectra web site in April, 2018).

Barani, S., D. Spallarose, P. Bazzurro & C. Eva (2007). Sensitivity analysis of seismic hazard for Western Liguria (North Western Italy): A first attempt towards the understanding and quantification of hazard uncertainty. Tectonophysics 435(1-4), 13-35.

Beauval, C. and O. Scotti (2004). Quantifying sensitivities of PSHA for France to earthquake catalog uncertainties, truncation of ground-motion variability, and magnitude limits, BSSA 94 (5) 1579-1594.

Brune, J. N. (1999). Precarious rocks along the Mojave section of the San Andreas fault, California: Constraints on ground motion from great earthquakes, Seism. Res. Lett. 70 (1), 29-33.

Biasi, G. and J. G. Anderson (2016). Disaggregating UCERF3 for Site-Specific Applications, Earthquake Spectra 32, 2009-2026.

Boore, D. M., Stewart, J. P., Seyhan, E., and Atkinson, G. M. (2014). NGA-West2 equations for predicting PGA, PGV, and 5% damped PSA for shallow crustal earthquakes. Earthquake Spectra, 30(3):1057–1085.

Campbell, K. W. and Bozorgnia, Y. (2014). NGA-West2 ground motion model for the average horizontal components of PGA, PGV, and 5% damped linear acceleration response spectra. Earthquake Spectra, 30(3):1087–1115.

Chiou, B. S.-J. and Youngs, R. R. (2014). Update of the Chiou and Youngs NGA model for the average horizontal component of peak ground motion and response spectra. Earthquake Spectra, 30(3):1117–1153.

Field, E.H., Biasi, G.P., Bird, P., Dawson, T.E., Felzer, K.R., Jackson, D.D., Johnson, K.M., Jordan, T.H., Madden, C., Michael, A.J., Milner, K.R., Page, M.T., Parsons, T., Powers, P.M., Shaw, B.E., Thatcher, W.R., Weldon, R.J., II, and Zeng, Y., 2013, Uniform California earthquake rupture forecast, version 3 (UCERF3)—The time-independent model: U.S. Geological Survey Open-File Report 2013–1165, 97 p., California Geological Survey Special Report 228, and Southern California Earthquake Center Publication 1792, http://pubs.usgs.gov/of/2013/1165/.

Field, E. H., Arrowsmith, R. J., Biasi, G. P., Bird, P., Dawson, T. E., Felzer, K. R., Jackson, D. D., Johnson, K. M., Jordan, T. J., Madden, C., Michael, A. J., Milner, K. R., Page, M. T., Parsons, T., Powers, P. M., Shaw, B. E., Thatcher, W. R., Weldon, R. J. II, and Zeng, Y., 2014. Uniform California Earthquake Rupture Forecast Version 3 (UCERF3) - The timeindependent model, Bulletin of the Seismological Society of America 104, 1122–1180.

Grünthal, G. and R. Wahlström (2001). Sensitivity of parameters for probabilistic seismic hazard analysis using a logic tree approach, Journal of Earthquake Engineering, 5 (3), 309-328, DOI: 10.1080/13632460109350396.

Lee, Y., Hu, Z., Graf, W., and Huyck, C. (2018). Implementing the USGS 2014 NSHMP through robust simulation, Bull. Seism. Soc. Am. 108, .

Matan, A., M. Davis, O. Dor & R. Kamai (2017). The effect of alternative seismotectonic models on PSHA results – a sensitivity study for the case of Israel. Nat. Hazards Earth Syst. Sci., https://doi.org/10.5194/nhess-2017-281.

Molkenthin, C., F. Scherbaum, A. Griewank, N. Kuehn, P.J. Stafford & H. Leovey (2015). Sensitivity of probabilistic seismic hazard obtained by algorithmic differentiation: a feasibility study. Bulletin of the Seismological Society of America 105(3), 1810-1822.

Molkenthin, C., F. Scherbaum, A. Griewank, H. Leovey, S. Kucherenko and F. Cotton (2017). Derivative-based global sensitivity analysis: upper bound of sensitivities in seismic-hazard assessment using automatic differentiation, BSSA 107 (2), 984-1004, doi: 10.1785/0120160185.

Omang, A., P. Cummins, D. Robinson & S. Hidayati (2016). Sensitivity analysis for probabilistic seismic hazard analysis (PSHA) in the Aceh Fault Segment, Indonesia, in Cummins, P. R. & Meilano, I. (eds) Geohazards in Indonesia: Earth Science for Disaster Risk Reduction, Geological Society, London, Special Publications 441, http://doi.org/10.1144/SP441.5

Rabinowitz, N. and D. M. Steinberg (1991). Seismic hazard sensitivity analysis: a multi-parameter approach, BSSA 81, 796-817.

Rabinowitz, N. D. M. Steinberg and Gideon Leonard (1998). Logic trees, sensitivity analyses, and data reduction in probabilistic seismic hazard assessment, Earthquake Spectra 14 (1), 189-201.

Sabetta, F., A. Lucantoni, H. Bungum and J. J. Bommer (2005). Sensitivity of PSHA results to ground motion prediction relations and logic-tree weights, Soil Dynamics and Earthquake Engineering 25, 317-329.

USNRC (2012). "Practical Implementation Guidelines for SSHAC Level 3 and 4 Hazard Studies", NUREG-2117, US Nuclear Regulatory Commission, Washington D.C., USA.

Wesnousky, S. G., Bormann, J. M., Kreemer, C., Hammond, W. C., and Brune, J. N. (2012). Neotectonics, geodesy, and seismic hazard in the Northern Walker Lane of Western North America: Thirty kilometers of crustal shear and no strike-slip? Earth and Planetary Science Letters 329, 133–140.

Working Group on California Earthquake Probabilities (WGCEP) (2007). The Uniform California Earthquake Rupture Forecast, Version 2 (UCERF 2), U.S. Geol. Surv. Open-File Rept. 2007-1437.

Yazdani, A., A. Nickman, S.N. Eftekhari & E.Y. Dadras (2016). Sensitivity of near-fault PSHA results to input variables based on information theory. Bulletin of the Seismological Society of America 106 (4), 1858-1866, doi: 10.1785/0120160006.

7 Tables

Table 1: UCERF3 logic tree, showing only those properties for which multiple models have been used.

Property	Model	Weight	Number of Choices
Fault Geometry	FM3.1	0.5	2
	FM3.2	0.5	
Deformation Model	Geologic	0.3	4
	Ave Block Model	0.1	
	NeoKinema	0.3	
	Zeng	0.3	
Scaling Relationship	Shaw, 2013a, 2013b	0.2	5
	EllsworthB, WGCEP-2002	0.2	
	Hanks & Bakun, 2008	0.2	
	EllsworthB $\sqrt{L}$, Shaw,2013b	0.2	
	Shaw09mod Const $\Delta\tau$, Shaw, 2013b	0.2	
Slip Along Rupture	Tapered ($\sin^{1/2}$)	0.5	2
	Boxcar	0.5	
Total $M \geq 5$ Event Rate	6.5	0.1	3
	7.9	0.6	
	9.6	0.3	
$M_{max}^{off-fault}$	7.3	0.1	3
	7.6	0.8	
	7.9	0.1	
Off-Fault Spatial PDF	UCERF2 Smoothed Seis	0.5	2
	UCERF3 Smoothed Seis	0.5	

8 Figures
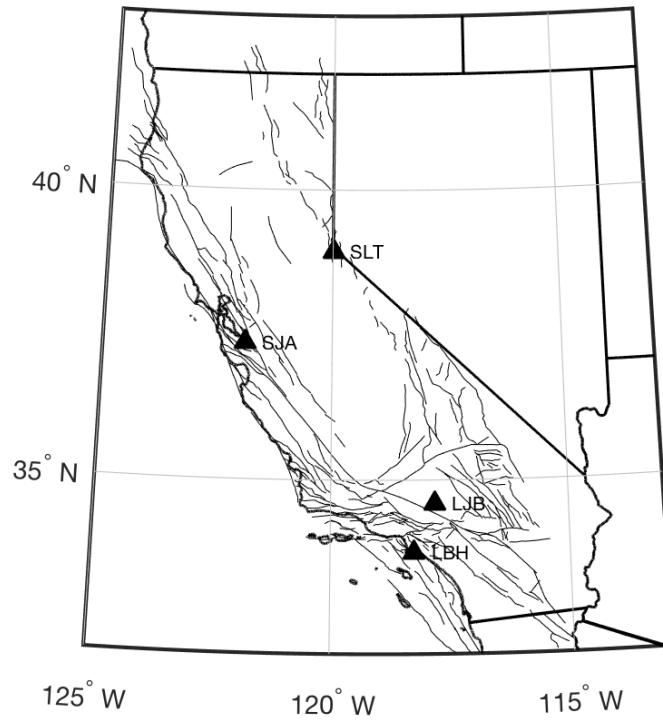
Figure 1: Map of California, showing faults included in the UCERF3 model 3.1, and locations of sites considered in this paper. Site initials are LBH- Long Beach Harbor, LJB - Lovejoy Buttes, SJA - San Jose Airport, and SLT - South Lake Tahoe.
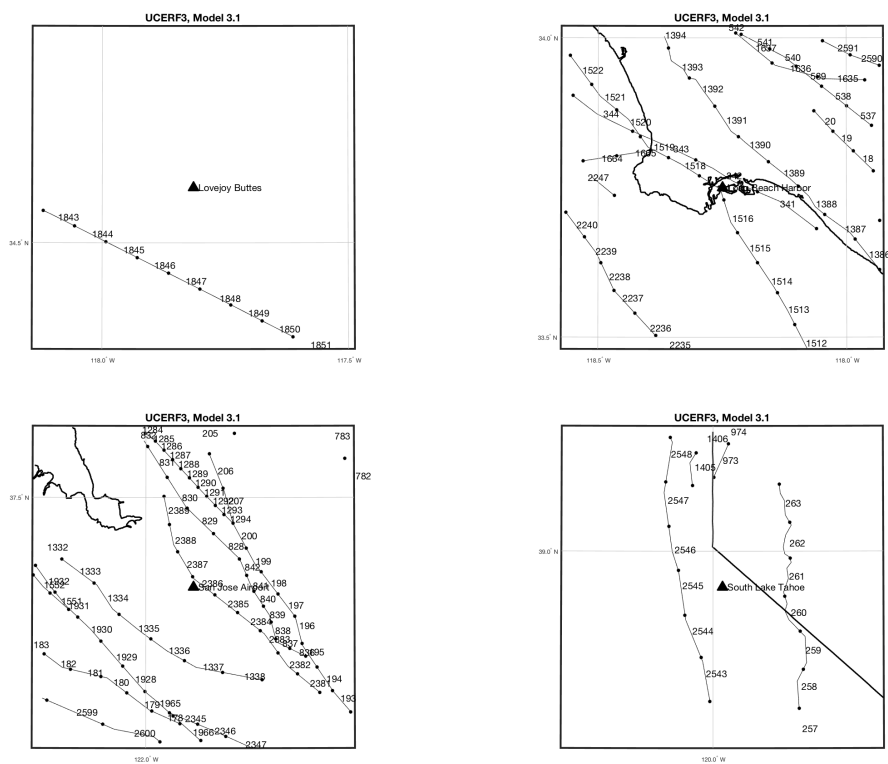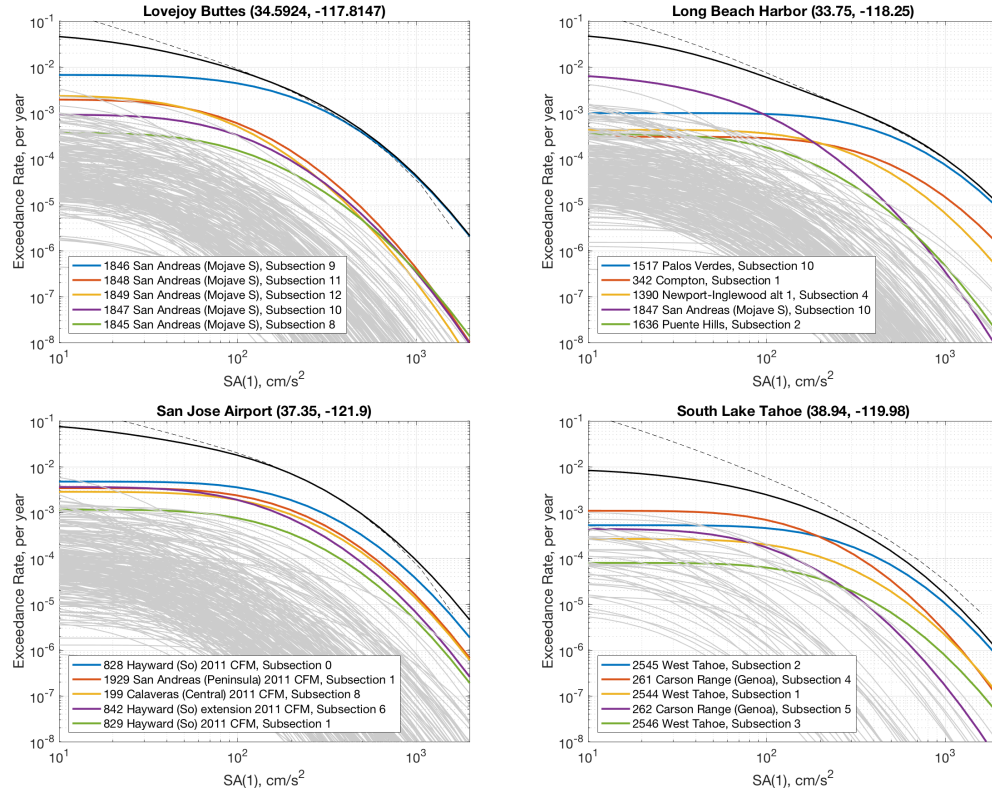
Figure 2: Location maps for the four sites.

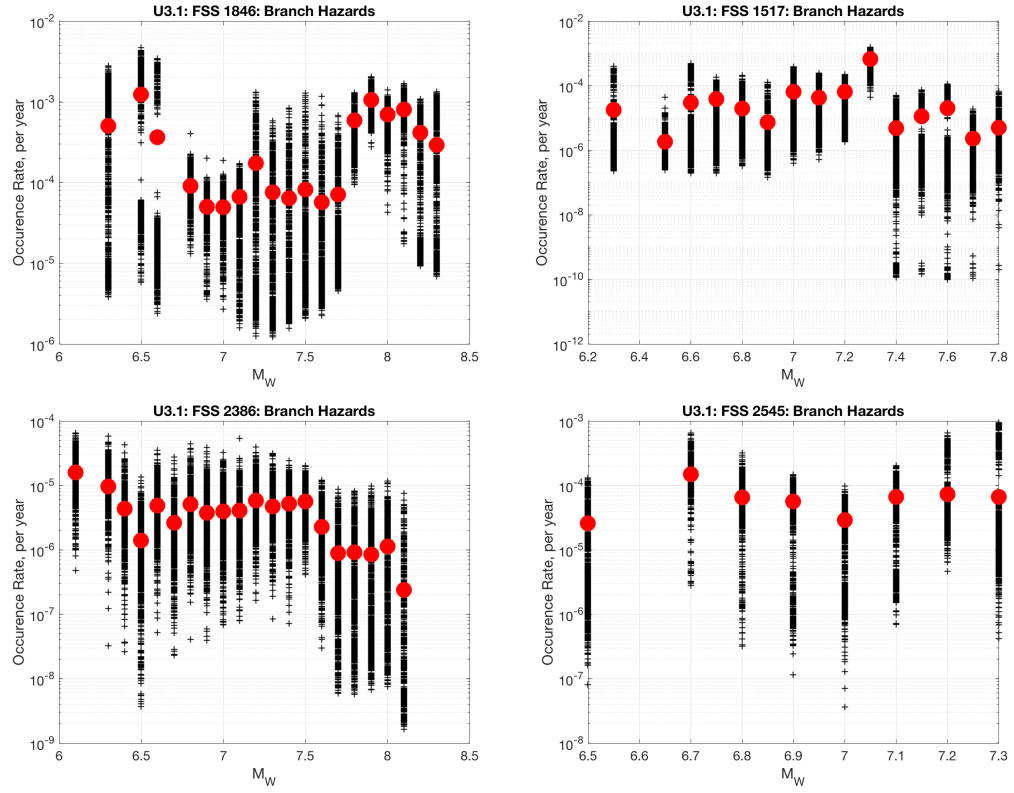Figure 3: Mean hazard curve contributions by subsection.

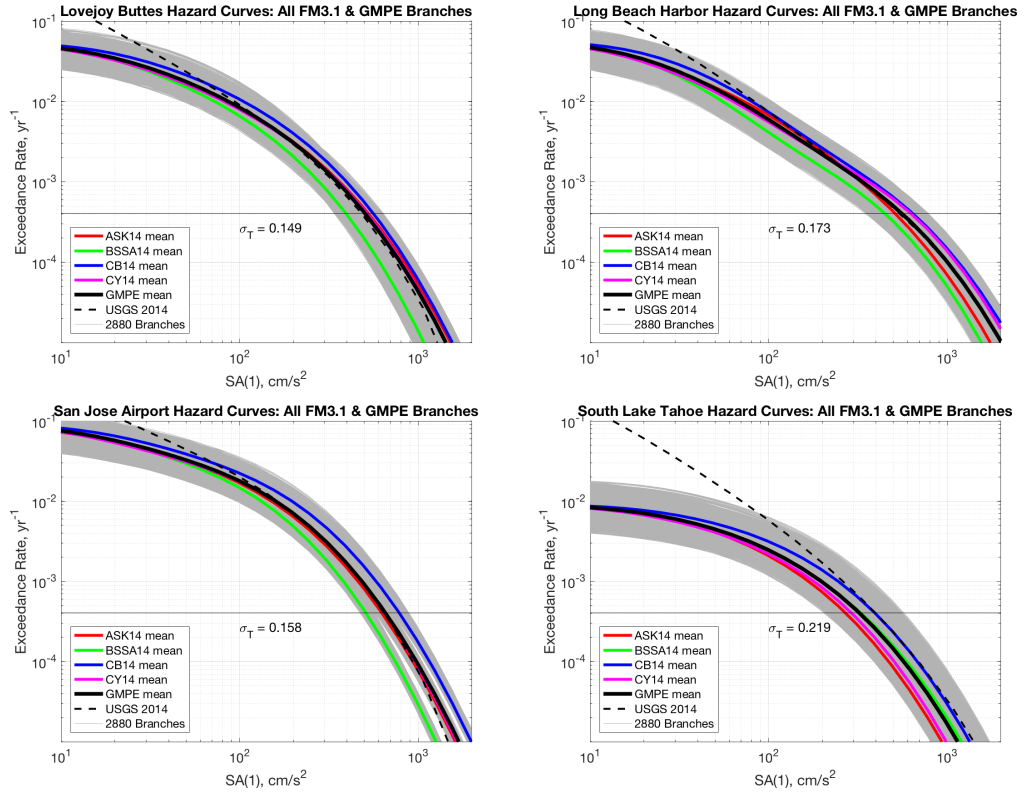Figure 4: Incremental magnitude - frequency distributions. The red points show the UCERF3.1 average rates.

Figure 5: Hazard curves for all 2880 branches of the logic tree.
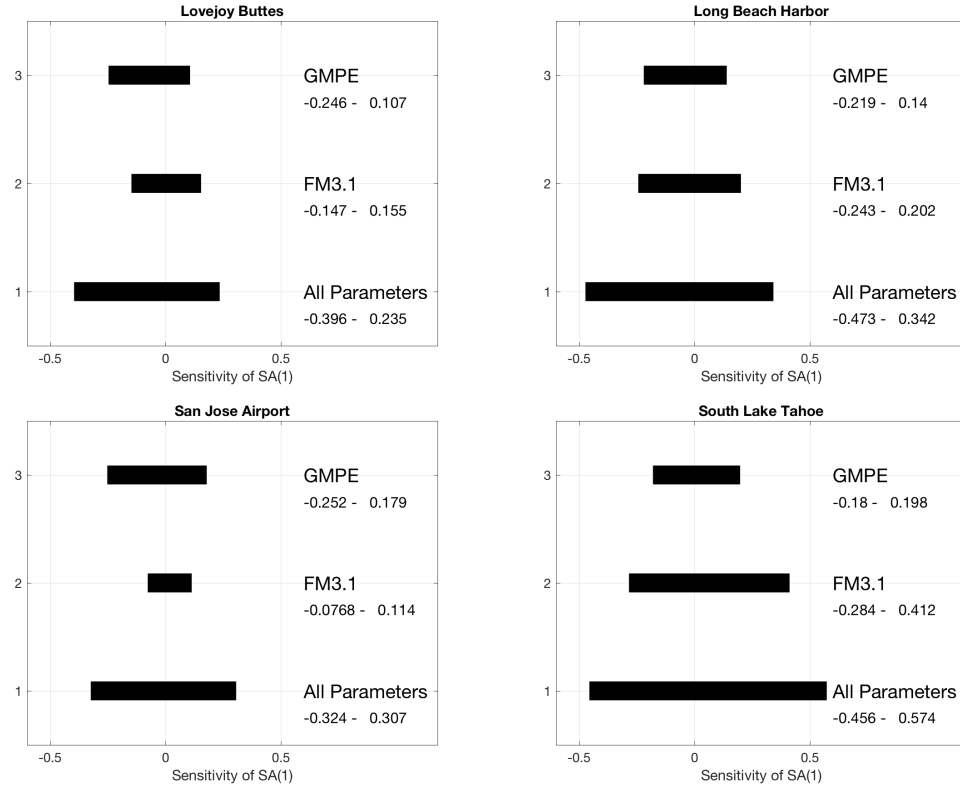
Figure 6: Tornado diagrams for SA(1 sec). Sensitivity is defined for an annual exceedance rate of $4.04 \cdot 10^{-4}$ per year. The range spans the natural log of the ratios of the smallest and largest hazard estimate to the mean of all branches. Numeric values are given to supplement the plot.

Lovejoy Buttes

GMPE
-0.22 - 0.0907

FM3.1
-0.122 - 0.118

All Parameters
-0.338 - 0.18

Sensitivity of SA(0.01)

Long Beach Harbor

GMPE
-0.263 - 0.113

FM3.1
-0.24 - 0.172

All Parameters
-0.503 - 0.308

Sensitivity of SA(0.01)

San Jose Airport

GMPE
-0.262 - 0.157

FM3.1
-0.0788 - 0.113

All Parameters
-0.333 - 0.276

Sensitivity of SA(0.01)

South Lake Tahoe

GMPE
-0.198 - 0.131

FM3.1
-0.255 - 0.351

All Parameters
-0.427 - 0.441

Sensitivity of SA(0.01)

Figure 7: Tornado diagrams showing the sensitivity of SA(0.01s), which is effectively peak acceleration. See caption to Figure 6 for more details.

17
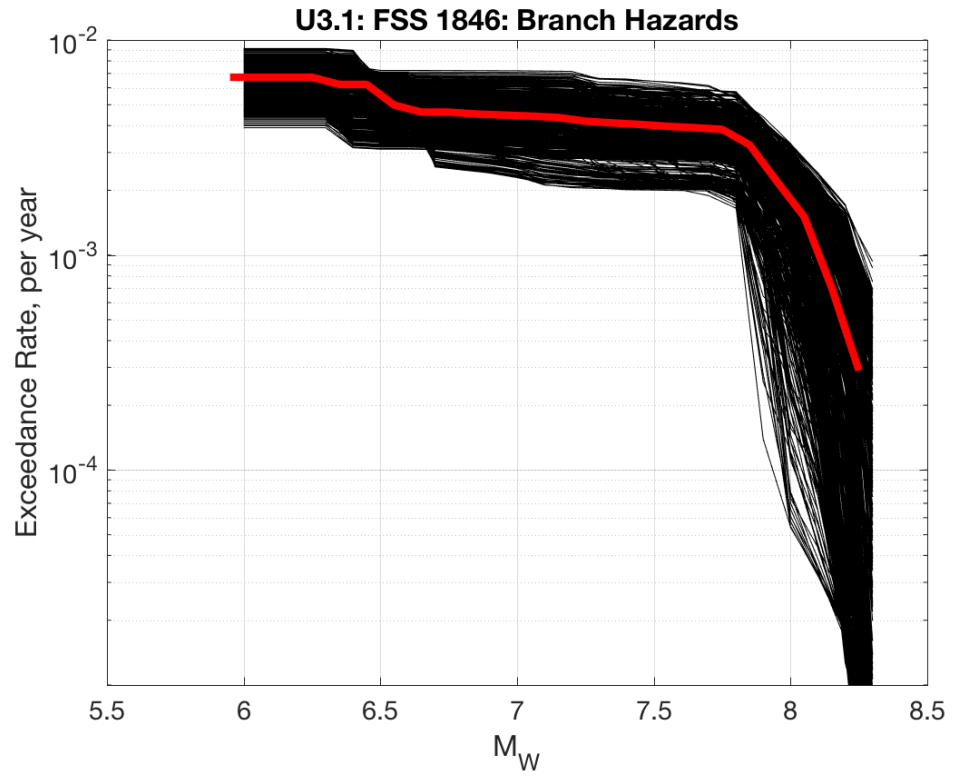
Figure 8: Cumulative magnitude - frequency distributions for Lovejoy Buttes from each of the 720 branches of the logic tree for FM3.1. The red points show the FM3.1 average rates.
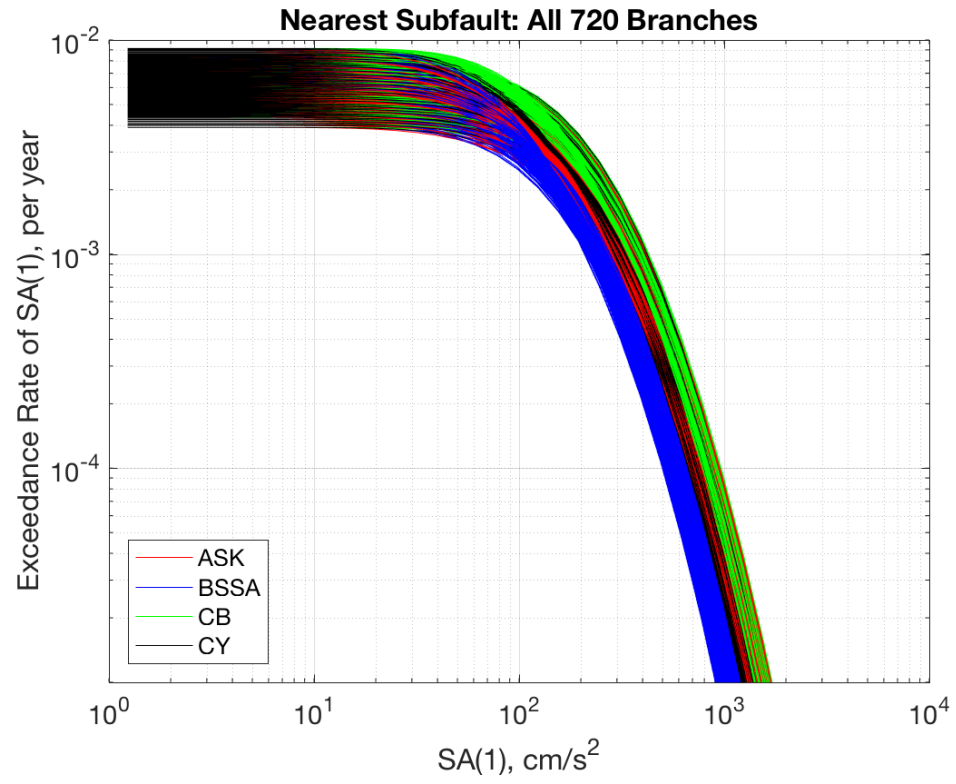
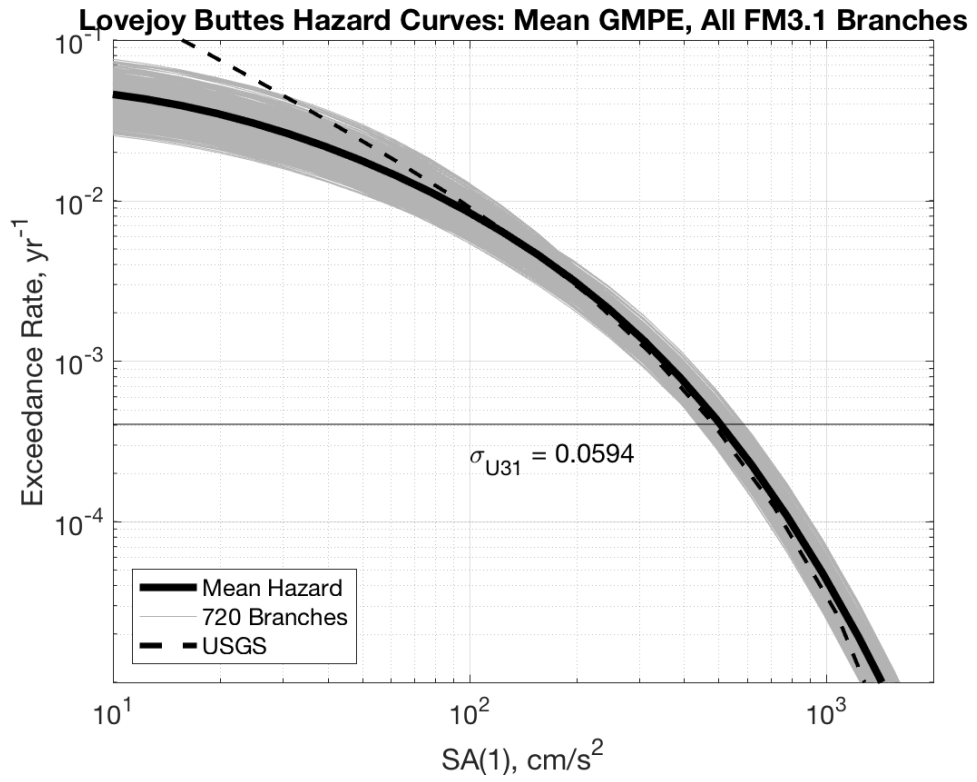Figure 9: Contribution of subfault 1846 of the San Andreas fault to the seismic hazard at Lovejoy Buttes.

Figure 10: Hazard curves at Lovejoy Buttes from all faults within 100 km, using the 720 UCERF3 logic tree branches generated with the mean GMPE.

Appendix B

UCERF3 Explorer 1: Software For Engineers

John G. Anderson and Glenn P. Biasi

August 19, 2018

1 Introduction

UCERF3 is the seismicity model used by CGS and USGS for the 2014 hazard model of California. It has been described by Field et al. (2014), and in even more detail by Field et al (2013). Prior California earthquake rupture forecasts (e.g. UCERF2) have been constructed from full-length faults or long fault segments that have been assumed to be the primary sources of large earthquakes. Earthquake occurrence rates for each fault are determined from physical constraints, such as the slip rate on the fault and recurrence intervals of large earthquakes in locations that have been trenched. UCERF3 has used a new concept of identifying a quarter to a third of a million possible earthquakes on the major faults, and then finding rates of each earthquake consistent with the physical constraints. While most of the rates in UCERF2 are fully determined (within uncertainties) by the constraints, in UCERF3, the rates are underdetermined, but the approach is a more realistic approximation to how the earthquake system actually works. The vast numbers of possible earthquakes in the UCERF3 model have resulted in difficulties for the engineering community to transition from the simple model to the more complex but realistic model. This software is aimed at providing products for engineers that will make the transition somewhat easier.

2 Concept of UCERF3

3 Software

3.1 Provided Data Files

u31rups.mat and u32rups.mat are Matlab structures with one entry for each rupture event. Data provided are rupture id number, magnitude, occurrence rate in the average model, and a list of fault subsections that are included in this rupture.

u31ss and u32ss are Matlab structures with one entry for each fault subsection, for UCERF3 model 3.1 and 3.2 respectively.

u31ssx and u32ssx are Matlab structures that include everything from u31ss and u32ss, respectively. Added to these for each fault subsection is a list of each of the ruptures that use this subsection: rupture id number (rupid), magnitude (rmag) and rate (rrate) are added to the structure. Magnitudes and rates are the UCERF3 average for models 3.1 and 3.2, respectively.

u31ssy and u32ssy are Matlab structures that include everything from u31ss and u32ss, respectively. Added to these for each fault subsection is the average S3MFD as defined by Biasi and Anderson (2016). The magnitudes are given in bins (hmag), in which the rates (s3mfd) combine the rates of all events added in u31ssx with magnitudes in that magnitude bin. With the accumulation of information, there is no additional need for u31ss or u31ssx.

3.2 Generated Data Files

u31fsshaz. This preserves the hazard curves at the site for the fault subsection that is nearest to the site.

u31sitehaz1. This contains a subset of the fault subsections in u31ssy, ordered by distance to the site. Several fields are added that are not in u31ssy:

sitename, slat, slong give the site name and location.

rx gives the distance from the site to the top center of the fault (equal to rss)

brupid, bmag, brate - identify the ruptures id numbers, magnitudes, and rates of ruptures that first affect the site through this fault subsection.

3.3 Code

3.3.1 u3map

This is the primary code, that calls all the other functions in sequence.

In Matlab, edit this code to put in the site name, latitude, and longitude, and the period of hte desired response spectral hazard curve. Also one can change um from 1 to 2 to explore the output of ucerf3.2. The distance parameter rf=300 is standard, but can be decreased to save a little bit of computing time.

3.3.2 fssfinder(um,slat,slong,rf)

Output: Vectors used in later codes: kss,rss,kmin,rmin

Given the site location, this identifies all of the fault subsections within rf kilometers. The vectors kss an rss give the fault subsection id number and the distance. rss gives the distance from the subsection to the site. To be precise, rss is the distance from the site to a point near the center of the surface trace of the fault. It is found by the average of the coordinates defining the surface trace. So when more than two coordinates are used because the fault bends, this point will be near, but not at the center.

3.3.3 fssmap(um,sitename,slat,slong,rp,kss,rss,pt,pn)

Output: a map named U31map, which will be saved in the subdirectory Results. The map limits are rp kilometers north, south, east, and west of the site. For good resolution, a larger value of rp will generally lead to a map that is not very clear.

3.3.4 fsss3mfd_plt(um,kmin,pt,pn)

Output: plots of the magnitude - frequency relationship (S3MFD) as defined by Biasi and Anderson (1996) for the fault subsection kmin.

3.3.5 fsshaz(um)

Output: Matlab structure (e.g. u32fsshaz) and plot: (e.g. U32haz_fss2602T10.png). The structure saves hazard curves for the nearest fault subsection nearest to the site (e.g. UCERF 3.2, fault subsection id # 2602 in the example).

3.3.6 fss_sitehaz1(um,sitename,slat,slong,kss,rss)

Output: u31sitehaz1.
    Purpose - create a new structure out of u31ssy or u32ssy that
    1. Only contains the fault subsections that are needed for a specific site,
    2. The sequence of fault subsections is changed. In this structure, the sequence of substations is in order of increasing distance.
    3. Adds new fields (brupid, bmag, brate). These fields contain a subset of rupid, rmag, and rrate, which identify ruptures that do not also affect fault subsections that are % closer to the site than this one.
    This code can take a long time to run, as for each sequential fault subsection, it has to check all of the closer fault subsections to see if they have used ruptures that also appear in the current subsection.

3.3.7 fss_sitehaz2(um)

Output: u31sitehaz2
    Purpose generates a reduced subevent mfd, called b3mfd, that is formed from the same algorithm as s3mfd, but it only uses the ruptures that are identified by brupid, as included in the structure u31sitehaz1. The field b3mfd is added to u31sitehaz1, to create u31sitehaz2.

3.3.8 fss_sitehaz3(T)

Output: u31sitehaz3
    This code adds fields to u31sitehaz2 to generate a larger structure u31sitehaz3. For each subfault, it generates five hazard curves, for the input period T. The first four curves are generated for the distance from the fault subsection to the site, and using the GMPEs of ASK14 (ahask), BSSA14 (ahbssa), CB14, and CY14.

3.3.9   fss_sitehaz4

Output: Hazard curve for every fault subsection within 300 km of Lovejoy Butte.

Most of the hazard curves are shown in gray. The five that have the strongest contribution at about 0.25g are highlighted with color. The total hazard, which is the sum of all the other curves on the figure, is shown in black.

4   Sample Calculations

This will illustrate results for two sites.

4.1   Lovejoy Buttes

This site was considered by Biasi and Anderson (2016). Figure 1 shows a map of the site and nearby fault subsections, generated by fssmap. Within 30 km, the only fault is the San Andreas, as seen on this figure. Data for this figure is contained in the file u31ssy, so all that was needed to generate this figure in fssmap was to have the proper fault subsection identified, which was done by fssfinder.

Figure 2 shows the S3MFD for the primary subsection contributing to the hazard at LJB. Data for this figure is contained in the file u31ssy, so all that was needed to generate this figure in fsss3mfd_plt was to have the proper fault subsection identified, which was done by fssfinder.

Figure 3 shows that the four considered GMPEs give quite similar results for the hazard at LJB from the nearest fault subsection. This figure was prepared by fss_sitehaz1.

Figure 4 shows the contribution of every contributing fault subsection within 300 km for the site at LJB. The figure was generated by function fss_sitehaz4, following computations by all of the previous codes. The contributions from fss 1845, 1846, and 1847, and the total hazard curve, agree with the plot in Biasi and Anderson (2016). It is somewhat unexpected that fss 1848 and 1849 contribute as strongly as they do.

4.2   Long Beach Harbor.

Figures 5 to 8 are the equivalent, for Long Beach Harbor, of Figures 1 to 4 for Lovejoy Buttes. Comparing Figure 8 with the equivalent figure in Biasi and Anderson (2016), one can see that the five fault subsections that contribute most to the hazard represent five distinctly different faults. Those that were chosen for display in Biasi and Anderson agree with the curves in this figure.

5   Acknowledgements

contained in this document are those of the authors and should not be interpreted as necessarily representing the official policies, either expressed or implied, of the U.S. Government.

6 References

Biasi, G. and J. G. Anderson (2016). Disaggregating UCERF3 for Site-Specific Applications, Earthquake Spectra 32, 2009-2026.

Field, E.H., Biasi, G.P., Bird, P., Dawson, T.E., Felzer, K.R., Jackson, D.D., Johnson, K.M., Jordan, T.H., Madden, C., Michael, A.J., Milner, K.R., Page, M.T., Parsons, T., Powers, P.M., Shaw, B.E., Thatcher, W.R., Weldon, R.J., II, and Zeng, Y., 2013, Uniform California earthquake rupture forecast, version 3 (UCERF3)—The time-independent model: U.S. Geological Survey Open-File Report 2013–1165, 97 p., California Geological Survey Special Report 228, and Southern California Earthquake Center Publication 1792, http://pubs.usgs.gov/of/2013/1165/.

Field, E. H., Arrowsmith, R. J., Biasi, G. P., Bird, P., Dawson, T. E., Felzer, K. R., Jackson, D. D., Johnson, K. M., Jordan, T. J., Madden, C., Michael, A. J., Milner, K. R., Page, M. T., Parsons, T., Powers, P. M., Shaw, B. E., Thatcher, W. R., Weldon, R. J. II, and Zeng, Y., 2014. Uniform California Earthquake Rupture Forecast Version 3 (UCERF3) - The timeindependent model, Bulletin of the Seismological Society of America 104, 1122–1180.
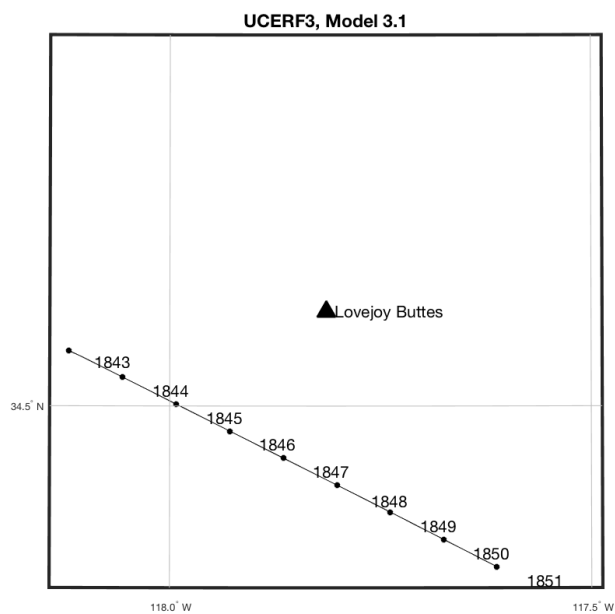
7 Figures
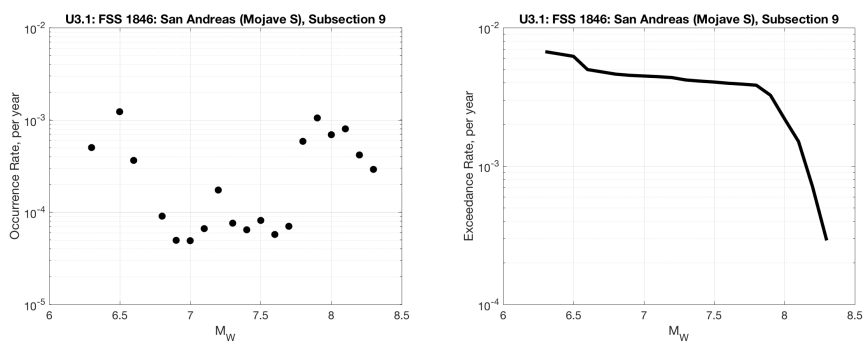

Figure 1: Map, site and nearby fault subsections.
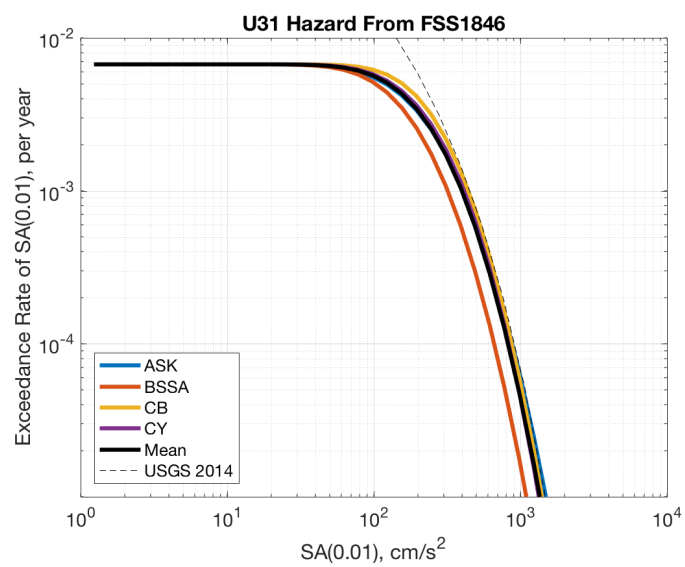

Figure 2: s3mfd for section 1846

Figure 3: Hazard at LJB from 1846 - sensitivity to GMPE

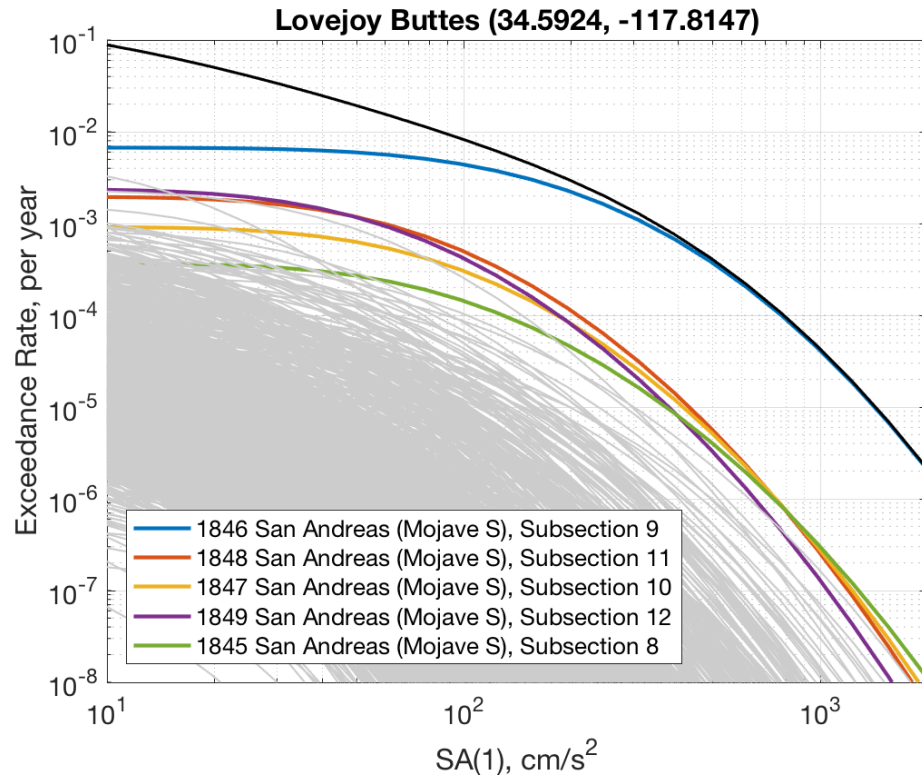Figure 4: Full hazard at LJB. Contributions from other subsections.

Figure 5: Map, site and nearby fault subsections.

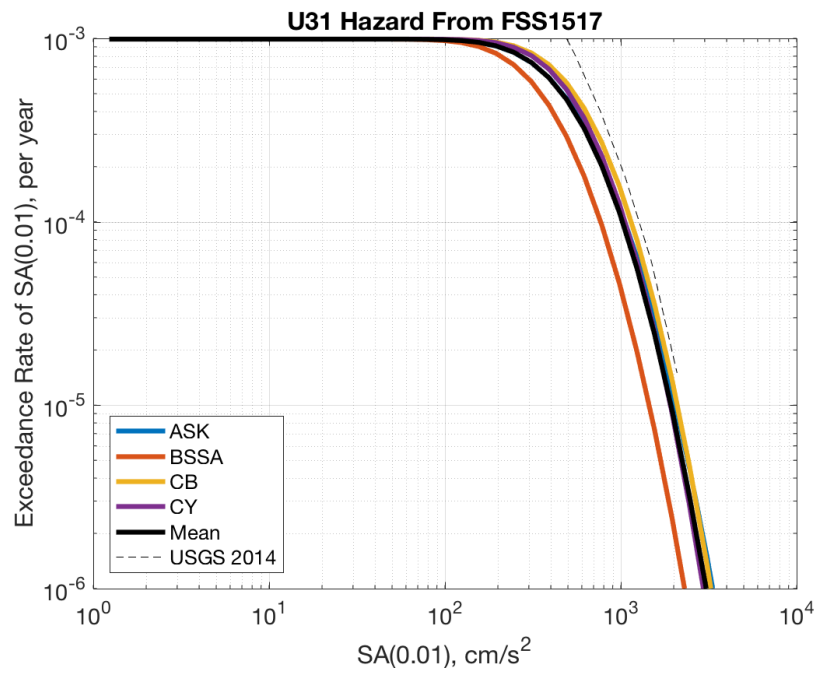Figure 6: Long Beach s3mfd for section 1517

9

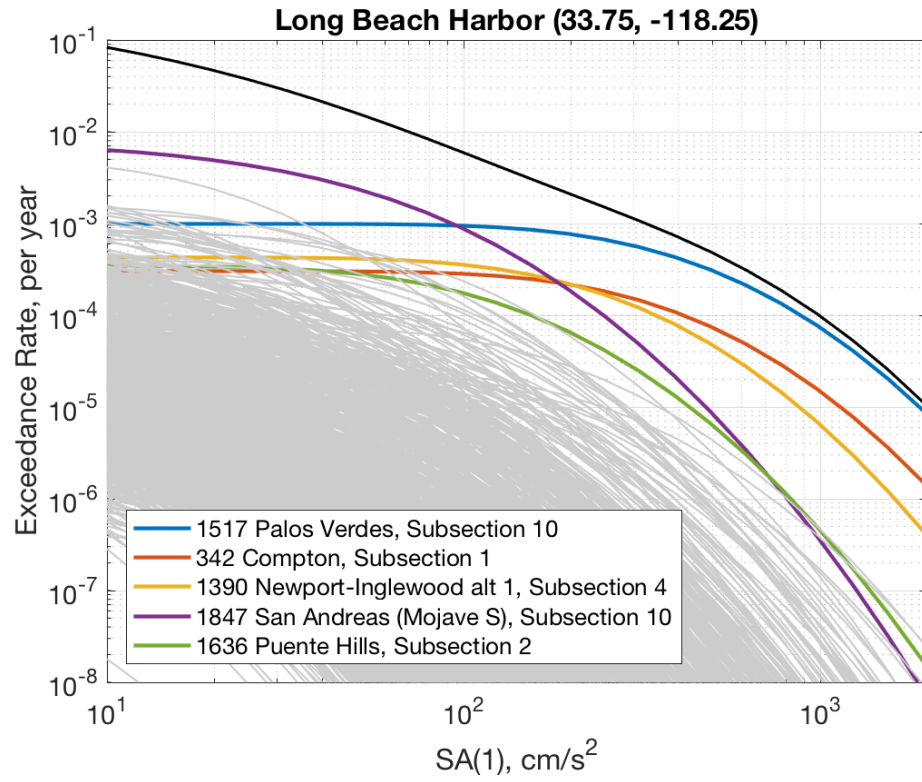Figure 7: Hazard at Long Beach Harbor from 1517 - sensitivity to GMPE

Figure 8: Full hazard at Long Beach. Contributions from other subsections.